Electronic Supplementary Material (ESI) for Catalysis Science & Technology.

Sulfidation of $MoO_3/\gamma\text{-}Al_2O_3$ towards highly efficient catalyst for CH_4 reforming with H_2S

Hao Wang[a], Jingxian Wu[a], Zhihuang Xiao[a], Zhejie Ma[a], Ping Li[a,*], Xinwei Zhang[b], Hongying Li[b], Xiangchen Fang[b]

[a] *State Key Laboratory of Chemical Engineering, East China University of Science and Technology, Shanghai 200237, China*
[b] *Dalian Petrochemical Research Institute, SINOPEC, Dalian 116045, Liaoning, China*

*Corresponding author.
E-mail address: lipingunilab@ecust.edu.cn (P. Li)

Supporting Information

Fig. S1 illustrates certain results of our previous study (Ref. [24]), which we obtained using AspenPlus software in light of the principle of minimum Gibbs free energy. The conditions set for reaction equilibrium calculation were 15 mol% H_2S and 0.1 MPa while changing the CH_4 molar fraction from 0 to 20 mol% (balanced with N_2) and the temperature from 400 to 1000 °C in a isothermal isobaric Gibbs reactor. Amorphous carbon was selected as a product of CH_4 dissociation. The results show that the addition of CH_4 can significantly increase the equilibrium conversion of H_2S, especially when the molar ratio of CH_4/H_2S is below the reformation stoichiometric ratio, i.e. 1/2. Furthermore, the increment greatly depends on reaction temperature, and high temperature is beneficial to H_2S conversion.

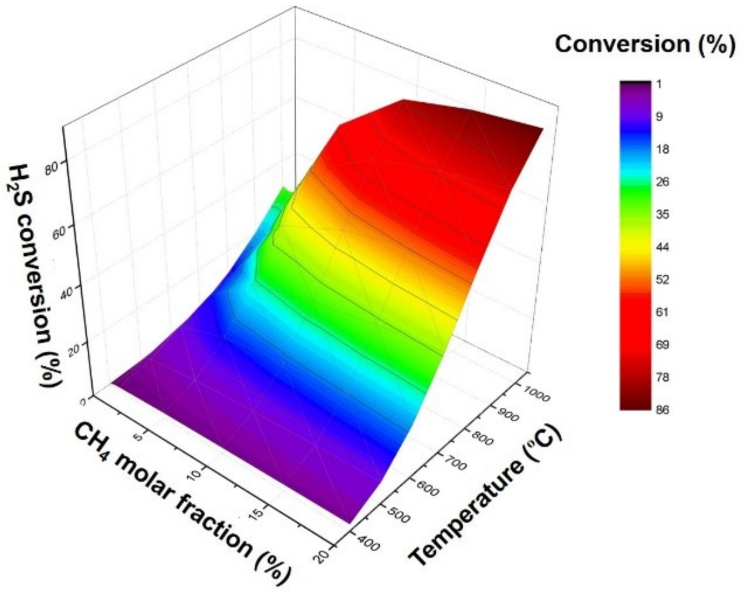

Fig. S1. Equilibrium conversion of 15 mol% H_2S as functions of CH_4 molar fraction (0 - 20 mol%) and temperature (400 – 1000 °C). Other conditions: 0.1 MPa in a isothermal isobaric Gibbs reactor, simulated using AspenPlus software based on the principle of minimum Gibbs free energy (Ref. [24]).

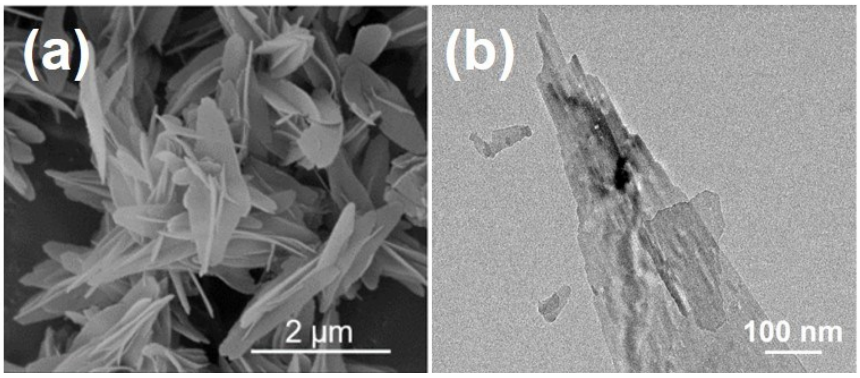

Fig. S2. Morphology of γ-Al_2O_3 synthesized. (a) SEM image showing clustered nanosheets architecture, and (b) typical TEM image of a piece of γ-Al_2O_3 nanosheet.

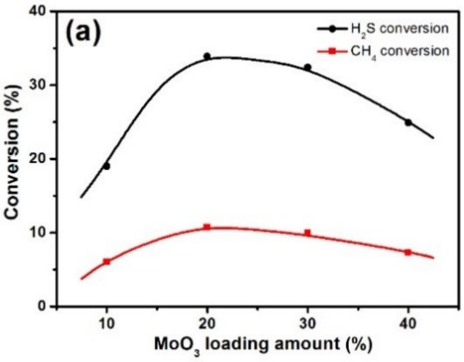

Fig. S3. Conversions of H_2S and CH_4 as a function of MoO_3 weight loading supported on γ-Al_2O_3 in CH_4/H_2S reforming process. Sulfidation condition: 600 °C, 1 h. Reaction conditions: $CH_4/H_2S/N_2$ = 1.5:1:7.5 (vol), 800 °C, 1 atm and GHSV = 20000 h^{-1}.

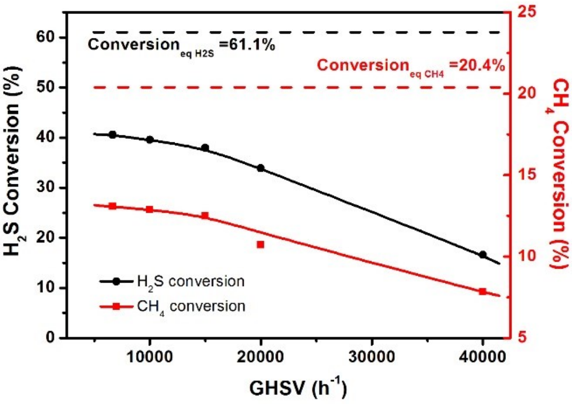

Fig. S4. Conversions of H_2S and CH_4 as a function of GHSV in CH_4/H_2S reforming process. Sulfidation condition: 600 °C, 1 h. Reaction conditions: $CH_4/H_2S/N_2$ = 1.5:1:7.5 (vol), 800 °C, 1 atm. Two dotted lines present the equilibrium conversions of CH_4 and H_2S under the corresponding conditions.

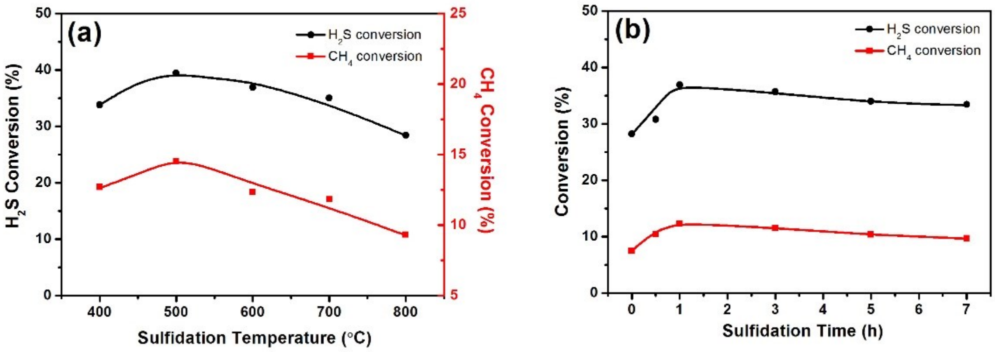

Fig. S5. Conversions of H_2S and CH_4 as a function of (a) sulfidation temperature and (b) time over 20 wt% MoO_3/Al_2O_3 catalyst (repetitive test for Figs. 1(a) and 5(a), respectively).

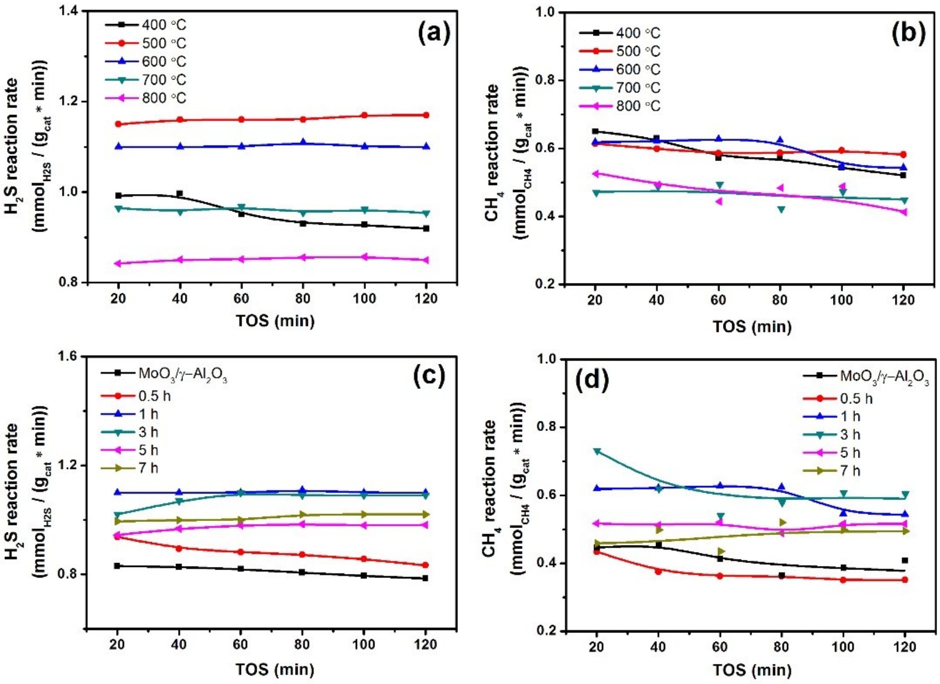

Fig. S6. Conversions of H_2S and CH_4 changing with the time on stream (TOS) in 2 h for the MoO_3/γ-Al_2O_3 catalyst sulfurized at different temperatures with 1 h (a, b) and sulfurized with different time at 600 °C (c, d).

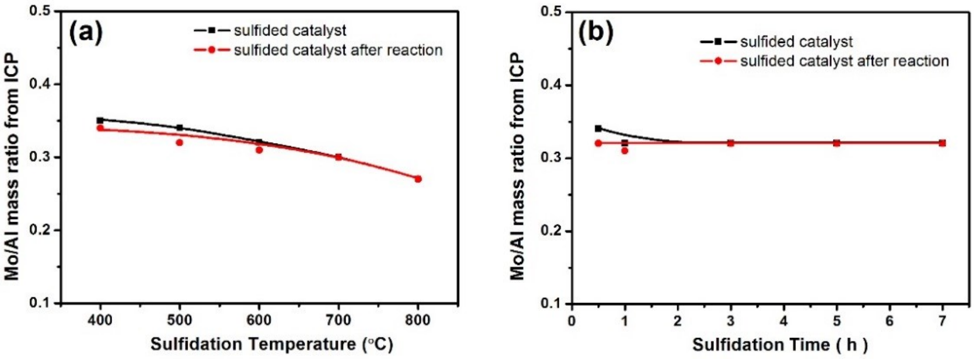

Fig. S7. Mo/Al mass ratio of sulfurized $MoO_3/\gamma\text{-}Al_2O_3$ catalyst before and after reaction as a function of (a) sulfidation temperature and (b) sulfidation time.

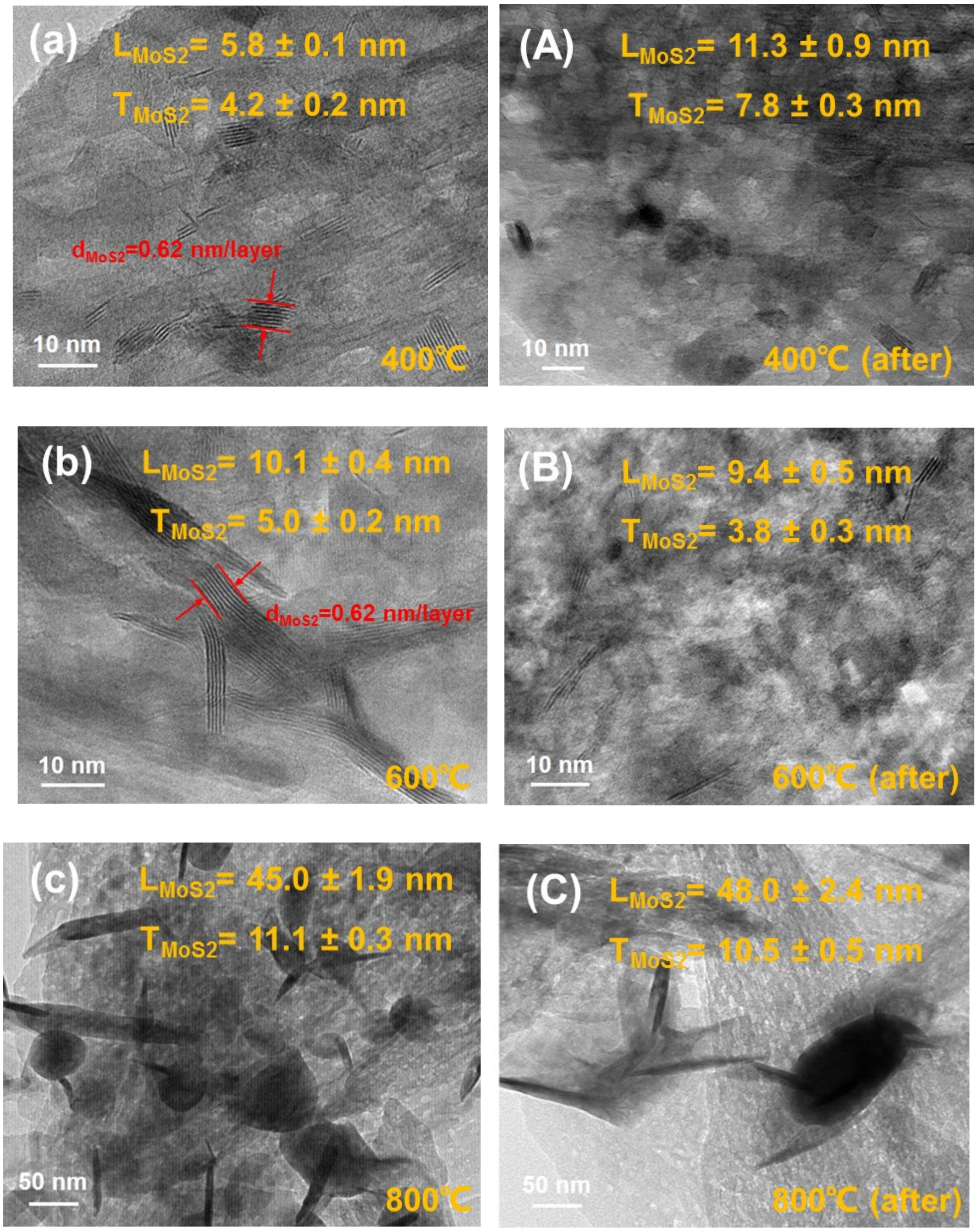
(a)
L$_{MoS2}$= 5.8 ± 0.1 nm
T$_{MoS2}$= 4.2 ± 0.2 nm
d$_{MoS2}$=0.62 nm/layer
10 nm
400℃
(A)
L$_{MoS2}$= 11.3 ± 0.9 nm
T$_{MoS2}$= 7.8 ± 0.3 nm
10 nm
400℃ (after)
(b)
L$_{MoS2}$= 10.1 ± 0.4 nm
T$_{MoS2}$= 5.0 ± 0.2 nm
d$_{MoS2}$=0.62 nm/layer
10 nm
600℃
(B)
L$_{MoS2}$= 9.4 ± 0.5 nm
T$_{MoS2}$= 3.8 ± 0.3 nm
10 nm
600℃ (after)
(c)
L$_{MoS2}$= 45.0 ± 1.9 nm
T$_{MoS2}$= 11.1 ± 0.3 nm
50 nm
800℃
(C)
L$_{MoS2}$= 48.0 ± 2.4 nm
T$_{MoS2}$= 10.5 ± 0.5 nm
50 nm
800℃ (after)

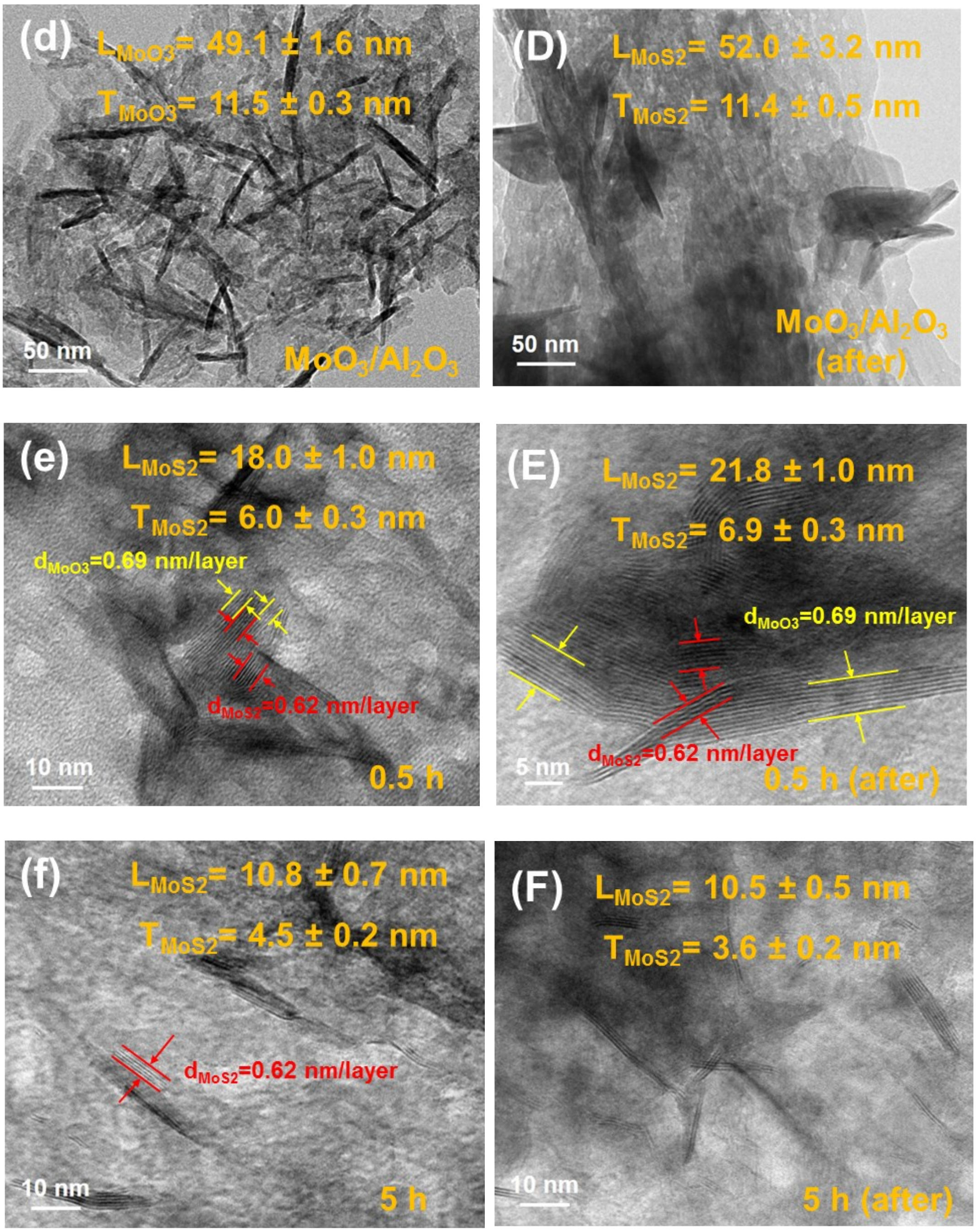

Fig. S8. TEM images of the $MoO_3/\gamma\text{-}Al_2O_3$ catalyst sulfurized at different temperatures with 1 h (a, b, c), the corresponding catalyst after the reaction (A, B, C), and sulfurized with different time at 600 °C (d, e, f), the corresponding catalyst after the reaction (D, E, F). The letter *L* represents the mean length of MoS_2 slabs and *T* is the mean thickness of MoS_2 slabs.

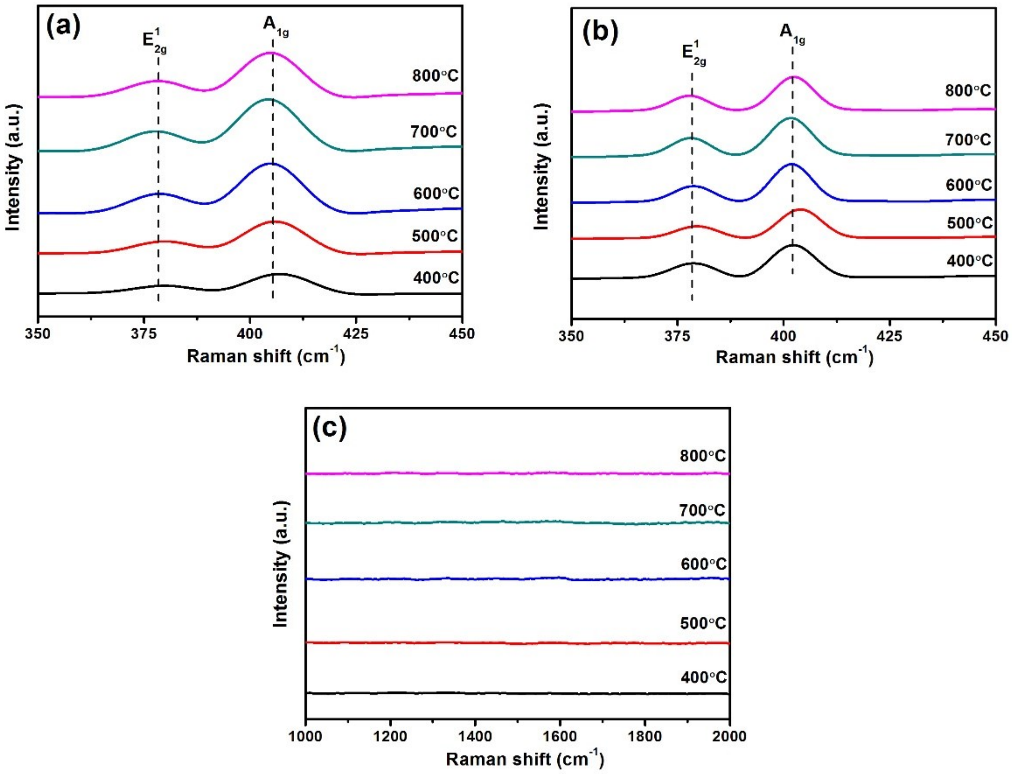

Fig. S9. Raman spectra of (a) 20 wt% MoO_3/Al_2O_3 after being sulfurized at different temperatures for 1 h, (b) the corresponding sulfurized samples after 2 h reaction test at 800 °C, and (c) the spectra in a range of 1000 – 2000 cm^{-1} for the samples of (b).

Table S1. Raman peak parameters of MoO_3/Al_2O_3 sample sulfurized at different temperatures before and after the reaction.

Sulfidation condition (temperature, time)	Sulfided catalyst				Sulfided catalyst after reaction			
	E^1_{2g} (cm^{-1})	A_{1g} (cm^{-1})	Difference (cm^{-1})	stacking number	E^1_{2g} (cm^{-1})	A_{1g} (cm^{-1})	Difference (cm^{-1})	stacking number
400 °C, 1 h	380.03	406.65	26.62	7	379.15	402.23	23.08	13
500 °C, 1 h	380.03	406.65	26.62	7	379.15	404.00	24.85	6
600 °C, 1 h	378.25	404.88	26.62	7	379.15	402.23	23.08	7
700 °C, 1 h	378.25	404.88	26.62	10	377.37	402.23	24.85	12
800 °C, 1 h	378.25	404.88	26.62	16	377.37	402.23	24.85	16

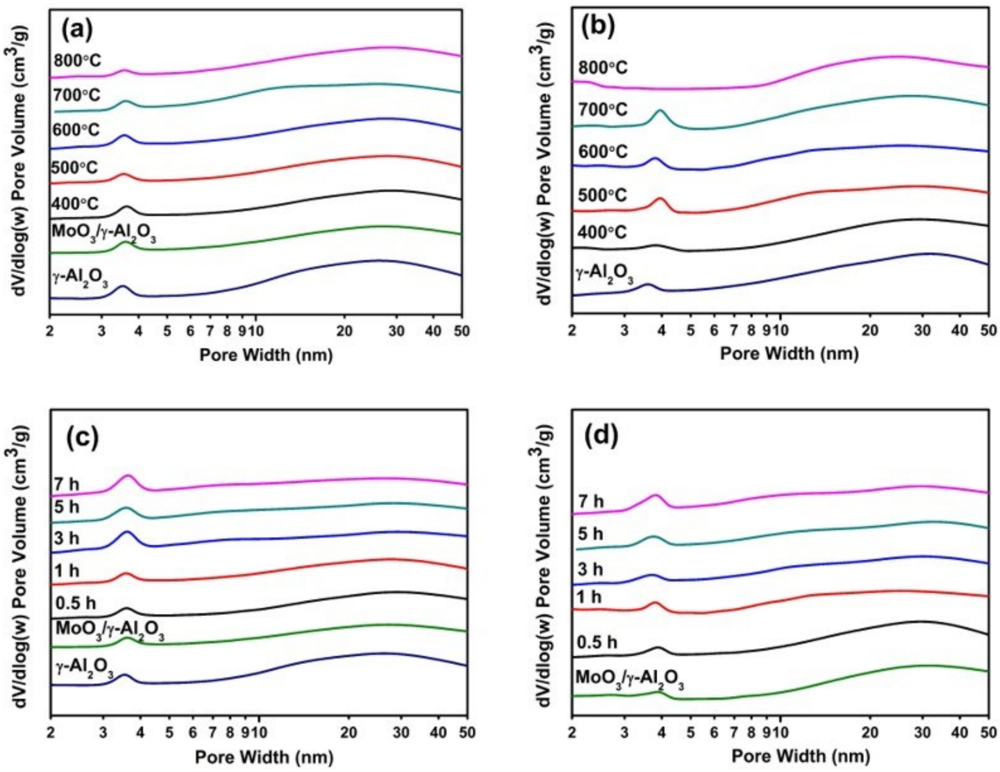

Fig. S10. The pore size distributions of (a, c) MoO_3/γ-Al_2O_3 after being sulfurized at different conditions, and (b, d) the corresponding sulfurized samples after 2 h reaction test at 800 °C. The pore size distributions of the untreated MoO_3/γ-Al_2O_3 sample before and after the reaction and the γ-Al_2O_3 support are also included.

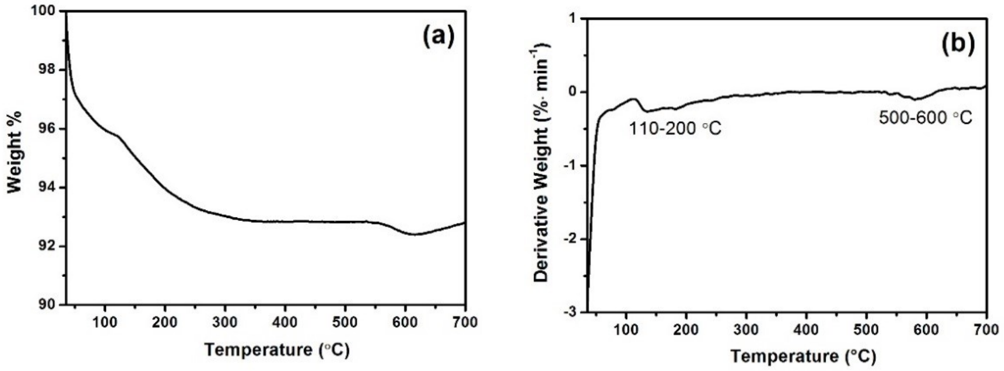

Fig. S11. (a) TGA curve and (b) corresponding DTG curve obtained under air flow for the γ-Al_2O_3 sample after reaction test at 800 °C for 2 h.

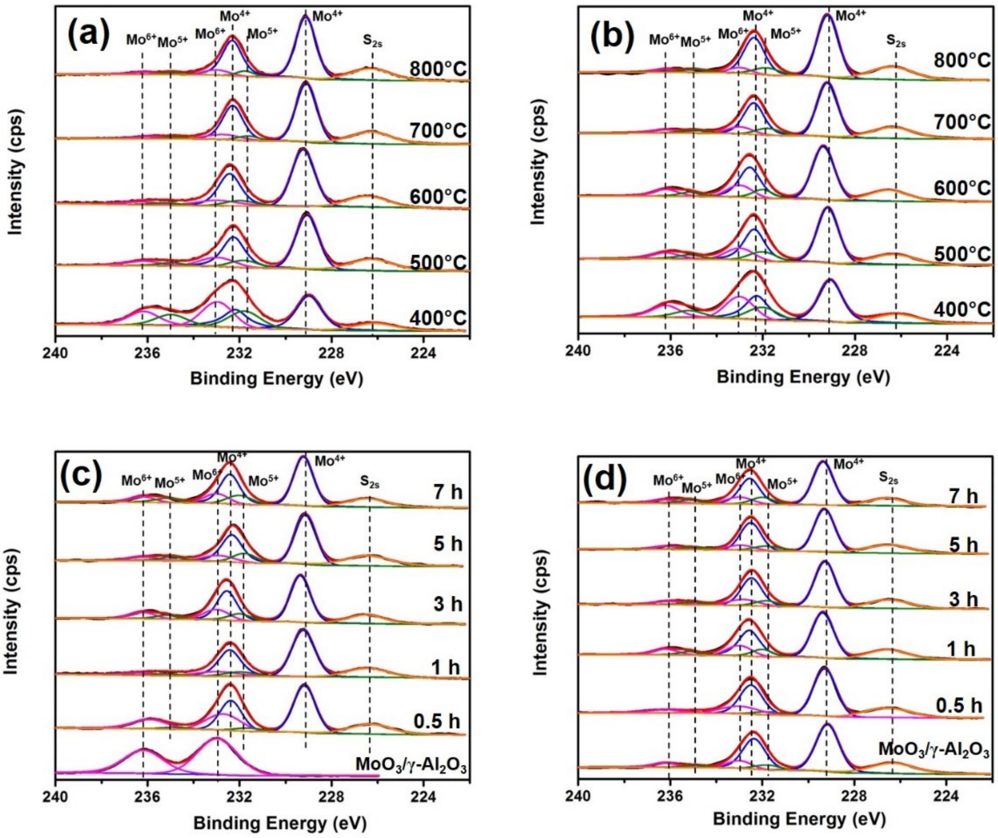

Fig. S12. XPS Mo 3d spectra of the MoO$_3$/γ-Al$_2$O$_3$ catalyst sulfurized at different temperatures with 1 h before (a) and after (b) the reaction, and sulfurized with different time at 600 °C before (c) and after (d) the reaction.

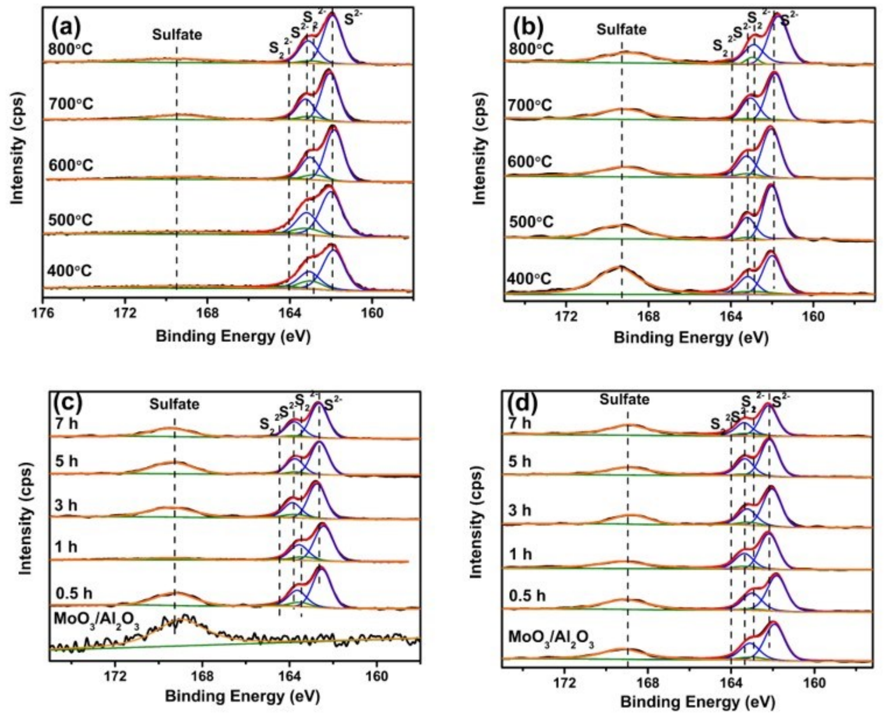

Fig. S13. XPS S 2p spectra of the $MoO_3/\gamma\text{-}Al_2O_3$ catalyst sulfurized at different temperatures with 1 h before (a) and after (b) the reaction, and sulfurized with different time at 600 °C before (c) and after (d) the reaction.

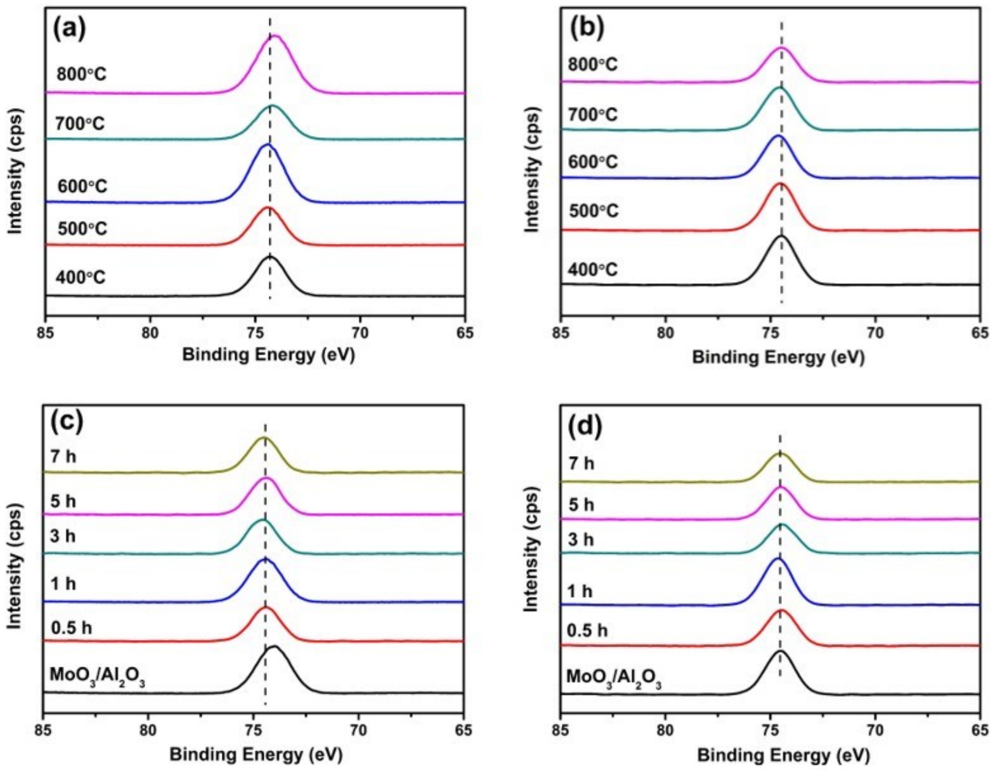

Fig. S14. XPS Al 2p spectra of the $MoO_3/\gamma\text{-}Al_2O_3$ catalyst sulfurized at different temperatures with 1 h before (a) and after (b) the reaction, and sulfurized with different time at 600 °C before (c) and after (d) the reaction.

Table S2. The catalytic performance of MoO_3/γ-Al_2O_3 sample sulfurized at optimal conditions and the results derived from citations for comparison.

Samples	Sulfidation condition	Reaction condition	Feed flow	Residence Time (GHSV)	Catalyst weight (volume)	H_2S conversion (%) and reaction rate (mmol/g_{cat}·min)	CH_4 conversion (%) and reaction rate (mmol/g_{cat}·min)	H_2 production rate (mmol/g_{cat}·min)	Ref.
MoO_3/Al_2O_3	100 ml/min, 20%H_2S/N_2, 500 °C, 1 h	800 °C, 1 atm	100 ml/min, $CH_4/H_2S/N_2$=1.5:1:7.5	0.24 s ($15000\ h^{-1}$)	0.16 g (0.4 ml)	39.7%, 1.16	13.2% 0.59	1.82	This study
MoO_3/Al_2O_3	100 ml/min, 20%H_2S/N_2, 600 °C, 1 h					37.9% 1.10	12.5% 0.54	1.73	
MoS_2	-	790 °C, 1 atm	180 ml/min, CH_4/H_2S=0.479:0.521	1.65 s	6.74 g (4.95 ml)	31.7%, 0.20	-	0.33	[17]
Mo/La_2O_3-ZrO_2	5.95 L/h H_2S /6.84 L/h N_2, 450 °C, 4 h	850 °C, 1 atm	0.189 L/h CH_4, 2.268 L/h H_2S	1.46 kg_{cat}·h/mol_{CH4}	3 g	44%, 0.93	97%, 0.18	-	[29]

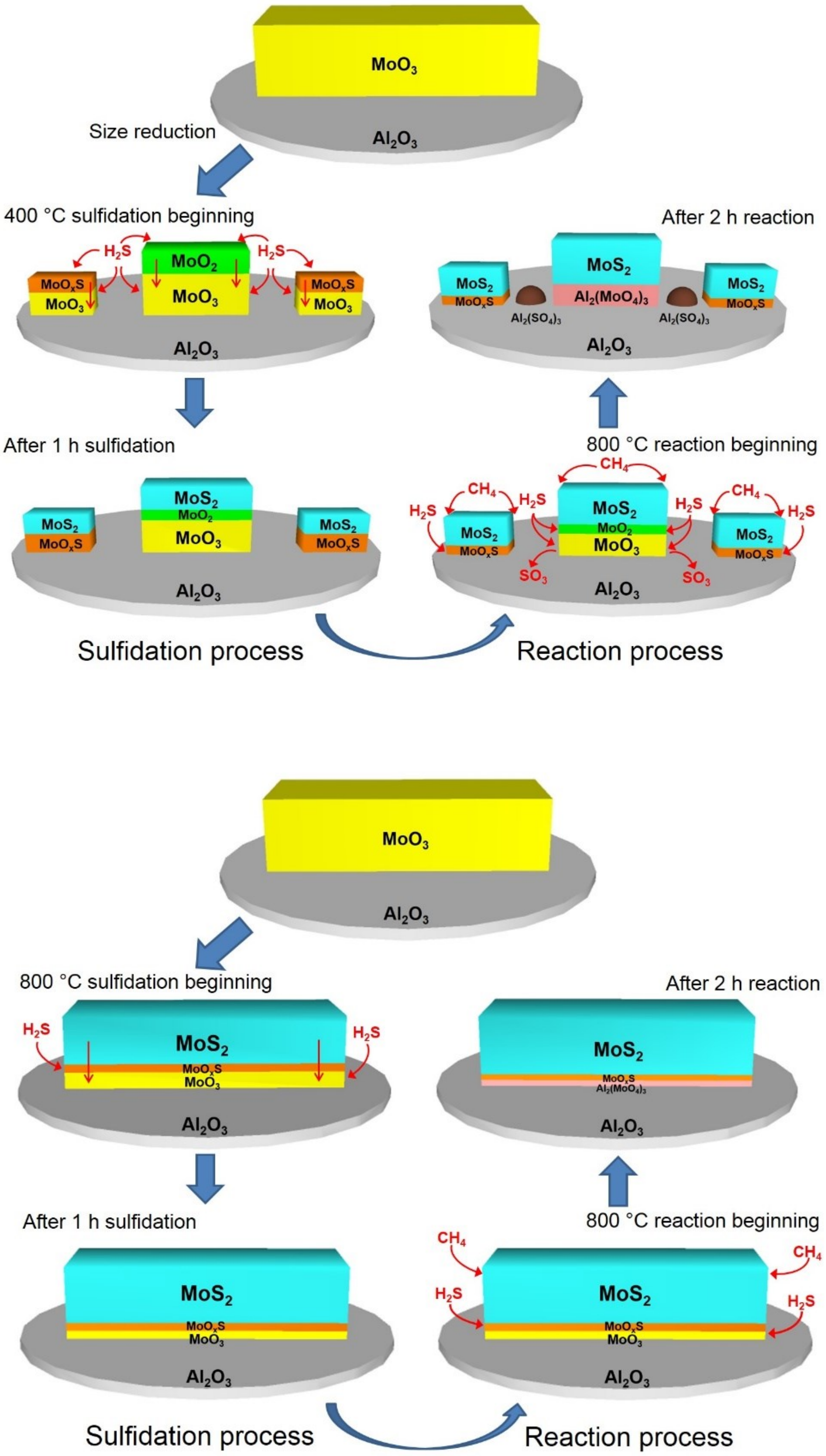

Fig. S15. Schematic illustration of substance transformation of $MoO_3/\gamma\text{-}Al_2O_3$ during the sulfidation at 400 °C (upper) or 800 °C (below) for 1 h followed by the reaction at 800 °C for 2 h.

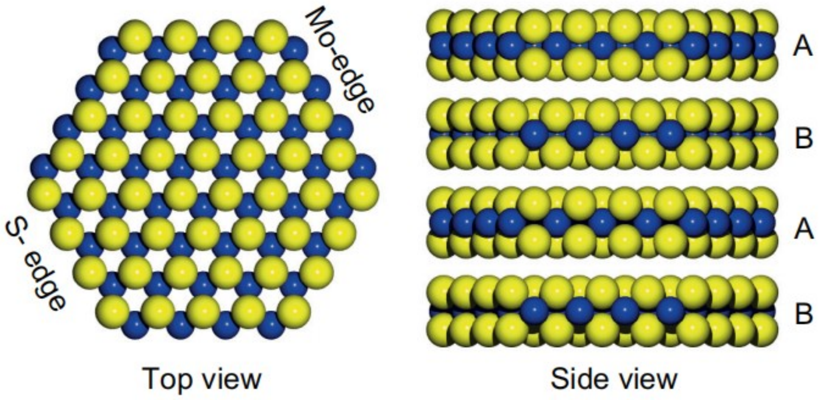

Fig. S16. The atomic model of the MoS_2 slab adopted from Refs. [71, 72] for edge Mo atom fraction calculation.

References

[17] S. K. Megalofonos and N. G. Papayannakos, *Int. J. Hydrogen Energy*, 1991, **16**, 319-327.

[24] Y. Y. Li, H. Gen, X. Cui, X. Liu, X. Z. Xie and P. Li, *Chem. Eng. Oil & Gas*, 2016, **45**, 32-37. (In Chinese)

[29] A. L. Martinez Salazar, J. A. Melo Banda, J. M. Dominguez Esquivel, V. H. Martinez Sifuentes, Y. Salazar Cerda, M. A. Coronel Garcia and M. A. Meraz Melo, *Int. J. Hydrogen Energy*, 2015, **40**, 17354-17360.

[71] J.V. Lauritsen, M.V. Bollinger, E. Lægsgaard, K.W. Jacobsen, J.K. Nørskov, B.S. Clausen, H. Topsøe, F. Besenbacher, *J. Catal.*, 2004, **221**, 510-522.

[72] A.S. Walton, J.V. Lauritsen, H. Topsoe, F. Besenbacher, *J. Catal.*, 2013, **308**, 306-318.